



# Ab initio calculations of optical absorption spectra: Solution of the Bethe–Salpeter equation within density matrix perturbation theory

Dario Rocca, Deyu Lu, and Giulia Galli

Citation: *J. Chem. Phys.* 133, 164109 (2010); doi: 10.1063/1.3494540

View online: <http://dx.doi.org/10.1063/1.3494540>

View Table of Contents: <http://jcp.aip.org/resource/1/JCPA6/v133/i16>

Published by the [American Institute of Physics](http://aip.org).

---

## Additional information on *J. Chem. Phys.*

Journal Homepage: <http://jcp.aip.org/>

Journal Information: [http://jcp.aip.org/about/about\\_the\\_journal](http://jcp.aip.org/about/about_the_journal)

Top downloads: [http://jcp.aip.org/features/most\\_downloaded](http://jcp.aip.org/features/most_downloaded)

Information for Authors: <http://jcp.aip.org/authors>

## ADVERTISEMENT

**physics today**

# Comment on any *Physics Today* article.

Measured energy in Japan

David von Seggern (vonseg@seismom.unr.edu) University of Nevada, Reno, Nevada 89557, USA

July 2012, page 10

DIGITAL OBJECT IDENTIFIER

<http://dx.doi.org/10.1038/PT.3.1619>

The article by Thorne Lay and Hiroo Kanamori (PT, 3, 1619) is an interesting one. The authors claim that the 1964 Chilean earthquake had approximately five times as much energy as a 100-megaton nuclear detonation event—a 50-megaton atmospheric explosion. This is not right. If the authors would have calculated the seismic moment–energy relationship between seismic moment and energy, they would find that the energy released in the Chilean earthquake was only about 1.5 times that of a 100-megaton nuclear explosion. The seismic energy release is approximately five times as much energy as a 100-megaton explosion, not a 50-megaton atmospheric explosion.

Despite the catastrophic damage potential of nuclear bombs, the forces of nature occasionally unleash much larger energy releases. However, by judicious preparation and avoidance measures, humans can significantly diminish the damage of natural events.

Comment on this article

By the act of hitting a ball with a bat, one calculates the force energy to deliver the ball to its new location, but one must also take into account that the ball extended its energy release to the ball which has been struck by the ball as its momentum passed and passed its energy to the struck item. Therefore the parameter of the damage extend into the future when the received energy to that item is pushed upon, later becomes released in a new event. Perhaps calculations of one added to that while another's calculations did not. E.Mc.

Written by Edgar McCarill, 14 July 2012 19:59

# Ab initio calculations of optical absorption spectra: Solution of the Bethe–Salpeter equation within density matrix perturbation theory

Dario Rocca,<sup>1,a)</sup> Deyu Lu,<sup>1,b)</sup> and Giulia Galli<sup>1,2</sup>

<sup>1</sup>Department of Chemistry, University of California, Davis, Davis, California 95616, USA

<sup>2</sup>Department of Physics, University of California, Davis, Davis, California 95616, USA

(Received 28 May 2010; accepted 8 September 2010; published online 27 October 2010)

We describe an *ab initio* approach to compute the optical absorption spectra of molecules and solids, which is suitable for the study of large systems and gives access to spectra within a wide energy range. In this approach, the quantum Liouville equation is solved iteratively within first order perturbation theory, with a Hamiltonian containing a static self-energy operator. This procedure is equivalent to solving the statically screened Bethe–Salpeter equation. Explicit calculations of single particle excited states and inversion of dielectric matrices are avoided using techniques based on density functional perturbation theory. In this way, full absorption spectra may be obtained with a computational workload comparable to ground state Hartree–Fock calculations. We present results for small molecules, for the spectra of a 1 nm Si cluster in a wide energy range (20 eV), and for a dipeptide exhibiting charge transfer excitations. © 2010 American Institute of Physics.

[doi:10.1063/1.3494540]

## I. INTRODUCTION

Spectroscopy is a key tool to characterize materials and nanostructures and the comparison of computed and measured spectra may greatly help interpret experimental data and validate theories and models.<sup>1–3</sup> In particular, knowledge of optical absorption spectra is of fundamental importance in many instances; for example, measurements and predictions of absorption spectra of candidate photoelectrodes are keys to understand how to optimize the absorption of sunlight by specific materials.<sup>4,5</sup> Unfortunately, in spite of important, recent progress,<sup>2</sup> the calculation of absorption spectra from first principles remains a challenging problem.

In the quantum chemistry community, optical absorption spectra are often computed with correlated methods such as coupled-cluster. These are limited to molecules with few atoms, especially if good quality basis sets are desired. The condensed matter physics community has mostly focused on time-dependent density functional theory (TDDFT)<sup>6</sup> and many-body perturbation theory (MBPT).<sup>2,7</sup> While TDDFT in the adiabatic local density approximation (LDA) and generalized gradient approximation (GGA) has been successfully applied to molecules and clusters, this theory may become inaccurate when electron-hole (e-h) interactions play an important role, e.g., in bulk insulators and semiconductors or in finite systems where charge transfer excitations are present. On the other hand, MBPT within a Green’s function formalism may describe excitation properties of both solids and molecules. Calculations using MBPT involve evaluating Kohn–Sham (KS) orbitals<sup>8</sup> and then applying self-energy corrections, for example, at the so called GW level<sup>9</sup> (G denotes the Green function and W the screened Coulomb inter-

action). The Bethe–Salpeter equation (BSE) may then be solved, e.g., starting from quasiparticle energies and wave functions.

Solving the BSE is considered the state-of-the-art approach to the computation of absorption spectra of bulk materials<sup>2,7,10,11</sup> and it has been applied to many systems, including silicon, germanium, diamond, GaAs, and LiF; in addition, several applications of the BSE to systems with reduced dimensionalities have appeared in the literature and these include graphene,<sup>12</sup> carbon and boron nitride nanotubes,<sup>13,14</sup> and finite systems, such as small sodium clusters and benzene and azobenzene molecules.<sup>15,16</sup>

Current techniques to solve the BSE use an electron-hole basis set and involve the computation of a multitude of single particle unoccupied states and the inversion of dielectric matrices.<sup>2,7</sup> Both operations may become prohibitively expensive, from a computational point of view, even for small molecules<sup>17</sup> and clusters, and their scaling as a function of the number of basis functions and of unoccupied states hamper the applicability of MBPT to nanostructured materials, e.g., for photovoltaic applications. It is therefore highly desirable to develop algorithms to solve the BSE that are scalable to large systems (e.g., containing hundreds of electrons) without resorting to approximations such as truncation of the number of unoccupied states and number of basis set functions.

Here we present a new approach to compute the absorption spectra of finite and periodic systems, based on the iterative solution of the quantum Liouville equation within first order perturbation theory, and with a Hamiltonian containing a static self-energy operator. Techniques based on density functional perturbation theory<sup>18</sup> (DFPT) are used to avoid inverting dielectric matrices<sup>19,20</sup> and explicit computation of single particle unoccupied orbitals.<sup>21,22</sup> This allows

<sup>a)</sup>Electronic mail: drocca@ucdavis.edu.

<sup>b)</sup>Present address: Center for Functional Nanomaterials, Brookhaven National Laboratory, Upton, New York 11973, USA.

for accurate and efficient calculations of absorption spectra with a workload comparable to ground state Hartree–Fock (HF) calculations.

The rest of the paper is organized as follows. In Sec. II, we derive the BSE within a density matrix formalism based on the linearized quantum Liouville equation and show how DFPT techniques can be used to avoid the explicit calculation of empty electronic states. In Sec. III, we discuss the technical details regarding the implementation of our method. In Sec. IV, our numerical implementation is validated against that of the YAMBO code,<sup>23</sup> a standard BSE code using an e-h basis set, for two small molecules H<sub>2</sub> and SiH<sub>4</sub> (Sec. IV A). Then we show the scalability of the method by computing the spectrum of a 1 nm silicon nanocluster (176 electrons) in a wide energy range (20 eV) (Sec. IV B). Finally, we present the study of charge transfer excitations (Sec. IV C) and discuss the first results for this kind of excitations obtained by solving the BSE. Section V contains our conclusions.

## II. METHOD

In optical absorption experiments, the intensity of the electromagnetic field of the incident light, which excites electrons from occupied to empty levels, is in general much weaker than that of internal fields, and thus can be treated within linear response theory. For a finite system, the absorption coefficient  $I(\omega)$  is proportional to the trace of the dynamical polarizability tensor  $\alpha_{ij}(\omega)$ :  $I(\omega) \propto \omega \operatorname{Im}(\operatorname{Tr}(\alpha(\omega)))$ . For solids, the optical absorption is given by the imaginary part of the macroscopic dielectric function  $\epsilon_2(\omega)$ . In the rest of this section, we will focus on the formulation for finite systems based on  $\alpha_{ij}(\omega)$ ; the generalization to periodic systems is presented in the Appendix.

Recently, an approach was proposed<sup>21,22</sup> to compute  $\alpha(\omega)$  by iteratively solving the time-dependent KS equations using DFPT, which was successfully applied to model systems containing hundreds of atoms.<sup>24–26</sup> Here we generalize such an approach to Hamiltonians containing static, nonlocal, self-energy operators, thus obtaining equations equivalent to the statically screened BSE. We then use iterative techniques to compute the eigenvalues and eigenvectors of the dielectric matrix entering the definition of the screened Coulomb interaction.<sup>19,20</sup> The starting point of our derivation is the quantum Liouville equation

$$i \frac{d\hat{\rho}(t)}{dt} = [\hat{H}(t), \hat{\rho}(t)], \quad (1)$$

where the square brackets indicate commutators and the hat denotes quantum-mechanical operators. Within a real space representation, the density matrix is given by  $\rho(\mathbf{r}, \mathbf{r}', t) = \sum_v \phi_v(\mathbf{r}, t) \phi_v^*(\mathbf{r}', t)$ , where  $\phi_v(\mathbf{r}, t)$  are single particle occupied orbitals. The time-dependent quasiparticle Hamiltonian in Hartree atomic units is

$$\begin{aligned} & \int \hat{H}(\mathbf{r}, \mathbf{r}', t) \phi(\mathbf{r}', t) d\mathbf{r}' \\ &= \left( -\frac{1}{2} \nabla^2 + v_H(\mathbf{r}, t) + v_{\text{ext}}(\mathbf{r}, t) \right) \phi(\mathbf{r}, t) \\ &+ \int \Sigma(\mathbf{r}, \mathbf{r}', t) \phi(\mathbf{r}', t) d\mathbf{r}', \end{aligned} \quad (2)$$

where  $v_{\text{ext}}$ ,  $v_H$ , and  $\Sigma$  are the external potential, Hartree potential, and the self-energy operator, respectively. We consider a static approximation to the self-energy and thus  $\Sigma$  depends on time only through the dependence on  $\hat{\rho}(t)$ .

The linearization of Eq. (1) with respect to  $v_{\text{ext}}$  leads to

$$\begin{aligned} i \frac{d\hat{\rho}'(t)}{dt} &= \mathcal{L} \cdot \hat{\rho}'(t) + [\hat{v}'_{\text{ext}}(t), \hat{\rho}^\circ], \\ \mathcal{L} \cdot \hat{\rho}'(t) &= [\hat{H}^\circ, \hat{\rho}'(t)] + [\hat{v}'_H[\hat{\rho}'](t), \hat{\rho}^\circ] + [\hat{\Sigma}'[\hat{\rho}'](t), \hat{\rho}^\circ], \end{aligned} \quad (3)$$

where variables with superscript “ $\circ$ ” represent unperturbed quantities and those with prime denote linear variations; specifically, in this case,  $\hat{\rho}' = \hat{\rho} - \hat{\rho}^\circ$  denotes the linear variation of the charge density. Note the dependence of  $\hat{v}_H$  and  $\hat{\Sigma}$  on the density matrix. In Eq. (3), a non-Hermitian operator  $\mathcal{L}$  acting on  $\hat{\rho}'$  has been defined, which is known as Liouvillian superoperator,<sup>21,22</sup> as its action is defined on a space of operators. By Fourier transforming Eq. (3) into the frequency domain, one obtains

$$(\omega - \mathcal{L}) \cdot \hat{\rho}'(\omega) = [\hat{v}'_{\text{ext}}(\omega), \hat{\rho}^\circ]. \quad (4)$$

The solution of this equation yields  $\hat{\rho}'(\omega)$ . The polarizability tensor  $\alpha$  is defined in terms of the components of the dipole moment  $d_i$  induced by a uniform external electric field  $\mathbf{E}$

$$d_i(\omega) = \sum_j \alpha_{ij}(\omega) E_j(\omega), \quad (5)$$

with  $v'_{\text{ext}}(\mathbf{r}, \omega) = -\mathbf{E}(\omega) \cdot \mathbf{r}$ . Since  $d_i(\omega) = \operatorname{Tr}(\hat{r}_i \hat{\rho}'(\omega))$ , the components of the polarizability tensor can be expressed as

$$\alpha_{ij}(\omega) = -\langle \hat{r}_i | (\omega - \mathcal{L} + i\eta)^{-1} \cdot [\hat{r}_j, \hat{\rho}^\circ] \rangle, \quad (6)$$

where  $\eta$  is a positive infinitesimal and we have written the scalar product of two operators  $A$  and  $B$  as  $\langle \hat{A} | \hat{B} \rangle \equiv \operatorname{Tr}(\hat{A}^\dagger \hat{B})$ .

The formalism introduced here is general and, in principle, can be applied using any approximation of the nonlocal and static self-energy operator,  $\Sigma(\mathbf{r}, \mathbf{r}')$ ; the effect of dynamical screening will be discussed in Sec. III. If  $\Sigma(\mathbf{r}, \mathbf{r}') = v_{\text{xc}}(\mathbf{r}) \delta(\mathbf{r} - \mathbf{r}')$ , where  $v_{\text{xc}}$  is the KS exchange-correlation potential, the adiabatic TDDFT formalism<sup>21,22</sup> is recovered. We now consider the case of the HF and of the static Coulomb-hole plus screened-exchange (COHSEX) approximations, yielding the following expressions for the self-energy operator ( $\Sigma_{\text{COHSEX}} = \Sigma_{\text{COH}} + \Sigma_{\text{SEX}}$ ):

$$\Sigma_{\text{HF}}(\mathbf{r}, \mathbf{r}', t) = - \sum_v \phi_v(\mathbf{r}, t) \phi_v^*(\mathbf{r}', t) v(\mathbf{r}, \mathbf{r}'), \quad (7)$$

$$\Sigma_{\text{COH}}(\mathbf{r}, \mathbf{r}') = \frac{1}{2} \delta(\mathbf{r} - \mathbf{r}') W_p(\mathbf{r}', \mathbf{r}), \quad (8)$$

$$\Sigma_{\text{SEX}}(\mathbf{r}, \mathbf{r}', t) = - \sum_v \phi_v(\mathbf{r}, t) \phi_v^*(\mathbf{r}', t) W(\mathbf{r}', \mathbf{r}), \quad (9)$$

where  $v(\mathbf{r}, \mathbf{r}')$  is the Coulomb kernel,  $W(\mathbf{r}', \mathbf{r}) = \int \epsilon^{-1}(\mathbf{r}', \mathbf{r}'') v(\mathbf{r}'', \mathbf{r}) d\mathbf{r}''$  is the statically screened Coulomb interaction,  $W_p = W - v$ , and  $\phi_v(\phi_c)$  denotes occupied (empty) states.  $\Sigma_{\text{HF}}$  and  $\Sigma_{\text{COHSEX}}$  can be easily linearized and inserted in Eq. (3). In the case of  $\Sigma_{\text{HF}}$ , the TDHF equations are obtained; in the case of  $\Sigma_{\text{COHSEX}}$ , we obtained so called TD-COHSEX equations. These are equivalent to the BSE with static screening in the electron-hole interaction and with quasiparticle corrections at the COHSEX level of theory.

The practical solution of Eq. (6) requires a basis set for  $\hat{\rho}'$ . A commonly used one is the ensemble of occupied and empty states of the unperturbed Hamiltonian, as the only nonzero matrix elements of  $\hat{\rho}'$  are those between unperturbed occupied and empty states:  $\langle \phi_c^\circ | \rho' | \phi_v^\circ \rangle$  and  $\langle \phi_v^\circ | \rho' | \phi_c^\circ \rangle$ .<sup>22</sup> Note that  $\langle \phi_v^\circ | [\hat{r}_j, \hat{\rho}^\circ] | \phi_v^\circ \rangle = \langle \phi_c^\circ | [\hat{r}_j, \hat{\rho}^\circ] | \phi_c^\circ \rangle = 0$ ,  $\forall v, v'$ , and  $c, c'$ ;  $\langle \phi_v^\circ | \hat{r}_i | \phi_v^\circ \rangle \neq 0$  and  $\langle \phi_c^\circ | \hat{r}_i | \phi_c^\circ \rangle \neq 0$ , however, one needs only the matrix elements  $\langle \phi_c^\circ | \hat{r}_i | \phi_v^\circ \rangle$  and  $\langle \phi_v^\circ | \hat{r}_i | \phi_c^\circ \rangle$  when computing the scalar product (trace) in Eq. (6).<sup>22</sup>

This so called e-h basis set is often used to solve TDHF equations and the BSE.<sup>2,7</sup> For spin singlet excitations of isolated systems, the operator  $\mathcal{L}$  takes the form<sup>2,7</sup>

$$\mathcal{L} = \begin{pmatrix} \mathcal{D} + 2\mathcal{K}^{1x} - \mathcal{K}^{1d} & 2\mathcal{K}^{2x} - \mathcal{K}^{2d} \\ -2\mathcal{K}^{2x*} + \mathcal{K}^{2d*} & -\mathcal{D} - 2\mathcal{K}^{1x*} + \mathcal{K}^{1d*} \end{pmatrix}, \quad (10)$$

where  $\mathcal{D}$ , the exchange terms  $\mathcal{K}^{1x}$  and  $\mathcal{K}^{2x}$ , and the direct terms  $\mathcal{K}^{1d}$  and  $\mathcal{K}^{2d}$  are defined as

$$\mathcal{D}_{vc, v' c'} = (\varepsilon_c^\circ - \varepsilon_v^\circ) \delta_{vv'} \delta_{cc'}, \quad (11)$$

$$\mathcal{K}_{vc, v' c'}^{1x} = \int \phi_c^{**}(\mathbf{r}) \phi_v^\circ(\mathbf{r}) \frac{1}{|\mathbf{r} - \mathbf{r}'|} \phi_{v'}^{**}(\mathbf{r}') \phi_{c'}^\circ(\mathbf{r}') d\mathbf{r} d\mathbf{r}', \quad (12)$$

$$\mathcal{K}_{vc, v' c'}^{2x} = \int \phi_c^{**}(\mathbf{r}) \phi_v^\circ(\mathbf{r}) \frac{1}{|\mathbf{r} - \mathbf{r}'|} \phi_{c'}^{**}(\mathbf{r}') \phi_{v'}^\circ(\mathbf{r}') d\mathbf{r} d\mathbf{r}', \quad (13)$$

$$\mathcal{K}_{vc, v' c'}^{1d} = \int \phi_c^{**}(\mathbf{r}) \phi_{c'}^\circ(\mathbf{r}) W(\mathbf{r}, \mathbf{r}') \phi_{v'}^{**}(\mathbf{r}') \phi_v^\circ(\mathbf{r}') d\mathbf{r} d\mathbf{r}', \quad (14)$$

$$\mathcal{K}_{vc, v' c'}^{2d} = \int \phi_c^{**}(\mathbf{r}) \phi_v^\circ(\mathbf{r}) W(\mathbf{r}, \mathbf{r}') \phi_{c'}^{**}(\mathbf{r}') \phi_v^\circ(\mathbf{r}') d\mathbf{r} d\mathbf{r}'. \quad (15)$$

In principle, the solution of Eq. (6) requires the calculation of the unoccupied single particle states of the unperturbed Hamiltonian and the matrix  $\mathcal{L}$  needs to be evaluated and stored explicitly. The need for an exceedingly large number of unoccupied states ( $\phi_c$ ) usually constitutes a bottleneck for calculations that require the evaluation of a large portion

of the spectrum and/or involve large systems; even for small molecules, obtaining converged spectra may be challenging in cases where the inclusion of many scattering states is necessary.<sup>17</sup>

In order to avoid explicit calculations of the empty states  $\phi_c^\circ$ , in the framework of DFPT we introduce projector operators onto the unperturbed empty state subspace  $\hat{Q} = \hat{I} - \hat{P} = \hat{I} - \sum_v |\phi_v^\circ\rangle\langle\phi_v^\circ|$ , where  $\hat{P}$  is the projector onto the occupied state subspace and  $\hat{I}$  is the identity operator; the evaluation of  $\hat{Q}$  requires the evaluation of the occupied states  $\phi_v^\circ$  only. Instead of using an electron-hole basis, we then represent the operators required to solve Eq. (6) ( $\rho'$ ,  $\hat{r}_i$ , and  $[\hat{r}_j, \hat{\rho}^\circ]$ ) within a so called *batch* representation.<sup>22</sup> For a generic operator  $\hat{A}$ , the batch representation is given by a vector whose  $2N_v$  components are defined in the following way:

$$|a_v\rangle = \hat{Q}\hat{A}|\phi_v^\circ\rangle, \quad (16)$$

$$\langle b_v| = \langle\phi_v^\circ|\hat{A}\hat{Q}, \quad (17)$$

where the index  $v$  runs from 1 to  $N_v$ ;  $N_v$  is the number of occupied states. To iteratively solve Eq. (6), we need to evaluate the action of the Liouvillian superoperator onto operators expressed within a batch representation. The action of the  $\mathcal{D}$  and  $\mathcal{K}$ 's on the components  $|a_v\rangle$  and  $|b_v\rangle$  of the batch representation of an operator  $\hat{A}$  is defined by

$$\mathcal{D}_{v, v'}|a_{v'}\rangle = (\hat{H}_{\text{COHSEX}}^\circ - \varepsilon_{v'}) \delta_{vv'}|a_{v'}\rangle, \quad (18)$$

$$\mathcal{K}_{v, v'}^{1x}|a_{v'}\rangle = \hat{Q} \left( \int \frac{1}{|\mathbf{r} - \mathbf{r}'|} \phi_{v'}^{**}(\mathbf{r}') a_{v'}(\mathbf{r}') d\mathbf{r}' \right) |\phi_v^\circ\rangle, \quad (19)$$

$$\mathcal{K}_{v, v'}^{2x}|b_{v'}\rangle = \hat{Q} \left( \int \frac{1}{|\mathbf{r} - \mathbf{r}'|} b_{v'}^{**}(\mathbf{r}') \phi_v^\circ(\mathbf{r}') d\mathbf{r}' \right) |\phi_v^\circ\rangle, \quad (20)$$

$$\mathcal{K}_{v, v'}^{1d}|a_{v'}\rangle = \hat{Q} \left( \int W(\mathbf{r}, \mathbf{r}') \phi_{v'}^{**}(\mathbf{r}') \phi_v^\circ(\mathbf{r}') d\mathbf{r}' \right) |a_{v'}\rangle, \quad (21)$$

$$\mathcal{K}_{v, v'}^{2d}|b_{v'}\rangle = \hat{Q} \left( \int W(\mathbf{r}, \mathbf{r}') b_{v'}^{**}(\mathbf{r}') \phi_v^\circ(\mathbf{r}') d\mathbf{r}' \right) |\phi_v^\circ\rangle. \quad (22)$$

If  $\hat{H}_{\text{COHSEX}}^\circ$  and  $W(\mathbf{r}, \mathbf{r}')$  are replaced by  $\hat{H}_{\text{HF}}^\circ$  and  $v(\mathbf{r}, \mathbf{r}')$ , respectively, one obtains the TDHF equations; these can be easily generalized to those of TDDFT for hybrid functionals. It is important to note that in this formulation, the calculation of  $\mathcal{K}^{1x}$ ,  $\mathcal{K}^{2x} \mathcal{K}^{1d}$ , and  $\mathcal{K}^{2d}$ , at variance from an e-h representation, involves a number of orbitals equal to the number of occupied states and for this reason, the required computational workload is comparable to that of ground state calculations.

In order to solve the BSE equation, one needs to evaluate the inverse dielectric matrix  $\epsilon^{-1}$  entering the definition of the self-energy, through the screened Coulomb interaction  $W$ . In principle, such an evaluation requires calculations of empty electronic states  $\phi_c$ . However, such computations can again be avoided by using techniques based on DFPT. In particular, following Refs. 19 and 20, we use an eigenvalue decomposition of the symmetrized dielectric matrix<sup>27</sup>  $\tilde{\epsilon}$  in

the random-phase approximation and an iterative algorithm to obtain eigenvalues and eigenvectors that only involves the evaluation of the action of  $\tilde{\epsilon}$  on trial potentials. Finally, no inversion of the dielectric matrix is necessary as  $\tilde{\epsilon}^{-1}$  is easily obtained from the eigenvalues ( $\lambda_i$ ) and eigenvectors ( $\tilde{v}_i$ ) of  $\tilde{\epsilon}$

$$\tilde{\epsilon}^{-1} = \hat{I} + \sum_{i=1}^N |\tilde{v}_i\rangle\langle\tilde{v}_i|(\lambda_i^{-1} - 1)\langle\tilde{v}_i|, \quad (23)$$

where  $\hat{I}$  indicates the identity operator. It has been shown that the eigenvalues  $\lambda_i$  are always greater than or equal to 1 (Ref. 27) and that for a variety of systems ( $\lambda_i^{-1} - 1$ ) decays rapidly to zero, as the eigenvalue index increases.<sup>19,20</sup> Therefore, the sum in Eq. (23) can be truncated to include just a small number of eigenvalues and eigenvectors, as discussed in Refs. 19 and 20 and shown below for several examples. In this way, the storage of the full dielectric matrix is avoided.

### III. ANALYSIS OF APPROXIMATIONS

In this section, we discuss the effects of several approximations used in the literature and this work, including the neglect of the coupling between resonant and antiresonant excitations (Tamm–Danoff approximation), dynamical screening effects, and the choice of the quasiparticle ground state wave functions.

#### A. Tamm–Danoff approximation

In the BSE, the Liouvillian operator  $\mathcal{L}$  is non-Hermitian, due to the coupling between resonant ( $a_v$ ) and antiresonant ( $b_v$ ) excitations present in the off-diagonal blocks in Eq. (10). In the literature,<sup>2,7,17,23,28–30</sup> Hermiticity is often enforced by neglecting the off-diagonal blocks of  $\mathcal{L}$ ; this is known as the Tamm–Danoff approximation (TDA).<sup>31</sup> The TDA greatly reduces the computational complexity of the BSE and it appears to accurately describe excitonic effects in solids, where it often yields a good agreement with experimental results.<sup>2,7,10,11,32,33</sup> For these reasons, the TDA has become a standard tool to study the optical absorption spectra of different materials.

However, the TDA does fail to account for plasmons, which are collective electronic excitations. An example of such a failure is the description of electron-energy loss (EEL) spectra of bulk silicon,<sup>34</sup> where both electron-hole pairs and antipairs need to be taken into account to capture plasmons. The effect of the TDA on the excitation spectra of molecular systems and nanostructures is much less understood than in solids. A negligible effect (of the order of 0.01 eV) has been observed on the lowest singlet and triplet excitation energies of simple molecules, e.g., SiH<sub>4</sub>;<sup>7</sup> on the other hand, recent calculations point to the breakdown of the TDA in describing some confined systems,<sup>35,36</sup> for example, carbon nanotubes.

Grüning *et al.*<sup>36</sup> reported that the TDA predicts a qualitatively wrong trend in the light polarization dependence of the absorption and EEL spectra of carbon nanotubes. Ma *et al.*<sup>35</sup> pointed out that the TDA can introduce an error of 0.4–0.5 eV with respect to the full BSE results in model chromophores. It is reasonable to expect that excitonic and plas-

monic excitations in finite systems are not as well separated in energy as in solids and their very distinction in the case of molecules may be difficult. Therefore, it is not surprising that the TDA fails for high energy excitations of carbon nanotubes, as well as for high energy excitations of 1 nm Si clusters, as we will see in Sec. IV B.

Since this work is focused on molecules and finite systems, we did not make use of the TDA. We used a generalized non-Hermitian Lanczos algorithm<sup>22</sup> to solve iteratively the full non-Hermitian BSE. Two coupled Lanczos chains for  $\mathcal{L}$  and  $\mathcal{L}^\dagger$  are iteratively computed starting from the same vector  $[\hat{r}_j, \hat{\rho}^\circ]$  in Eq. (6); the solution of the linear system  $(\omega - \mathcal{L} + i\eta)^{-1} \cdot [\hat{r}_j, \hat{\rho}^\circ]$  is then projected onto three left vectors  $\hat{r}_i$ , each one corresponding to a different polarization direction. In this way, all components of the polarizability tensor  $\alpha_{ij}(\omega)$  are computed from only three Lanczos iterative chains. We note that within the iterative approach adopted here, the calculation and storage of the full Liouvillian  $\mathcal{L}$  matrix are not required.

#### B. Dynamical screening effects

In principle, it is possible to extend the method within the static approximation presented in Sec. II to include dynamical screening effects in the BSE kernel. However, the solution of such a problem is computationally complex and demanding and it has not yet been addressed in our current implementation. Below we discuss possible effects of the static approximation on our results.

For valence excitations in solids, the static screening approximation is justified as long as the exciton binding energies are much smaller than plasma frequencies.<sup>2</sup> In molecular systems, the range of validity of the static screening approximation is not as well understood and very few results are available. In the case of SiH<sub>4</sub>, Rohlffing and Louie<sup>7</sup> found that the inclusion of the dynamical screening lowers the lowest excitation energy by about 0.1 eV. For the same system, Bechstedt *et al.* used the Shindo approximation<sup>37</sup> for the dynamical screening and found that a peak at about 10.6 eV obtained from the static BSE is blueshifted by about 0.2 eV.<sup>38</sup> In the case of biological chromophores, Ma *et al.* used a plasmon-pole model for  $\epsilon^{-1}(\omega)$  and first order perturbation theory to solve the dynamically screened BSE. They found that the inclusion of dynamical screening may lower the  $n \rightarrow \pi^*$  excitation energies by about 0.3 eV and the  $\pi \rightarrow \pi^*$  transitions by 0.1 eV.<sup>35</sup>

Given the very limited number of studies including dynamical screening, it is not yet possible to identify systematic errors introduced by the static approximation. However, we should bear in mind that the results presented in Sec. IV may be affected by errors of the same order of magnitude as those discussed in Refs. 7, 35, and 38 ( $\sim 0.1$ –0.3 eV).

#### C. Choice of the quasiparticle ground state wave functions

Within standard GW/BSE frameworks, the GW approximation is applied to compute a subset of quasiparticle energy levels (and orbitals) that are within the excitation energy range of interest, either nonself-consistently ( $G_0W_0$ ) or

self-consistently.<sup>39</sup> The BSE is subsequently solved for the e-h pairs defined within this subset. As shown in Eq. (18), within density matrix perturbation theory, one needs to compute the direct action of the quasiparticle Hamiltonian  $\hat{H}_{QP}^{\circ}$  on batches of orbitals [Eqs. (16) and (17)]. Consider the case where GW self-energy corrections have been performed for all the occupied states and some of the empty states up to a given number  $n_{cut}$ . For the rest of the empty states, we assume a rigid shift in the self-energy correction  $\Delta = \epsilon_{n_{cut}}^{QP} - \epsilon_{n_{cut}}^{KS}$ . The quasiparticle Hamiltonian is then given by

$$\begin{aligned} \hat{H}_{QP}^{\circ} = & \hat{H}_{KS}^{\circ} + \sum_{i=1}^{n_{cut}} (|\phi_i^{QP}\rangle \epsilon_i^{QP} \langle \phi_i^{QP}| - |\phi_i^{KS}\rangle \epsilon_i^{KS} \langle \phi_i^{KS}|) \\ & + \Delta \left( \hat{I} - \sum_{i=1}^{n_{cut}} |\phi_i^{QP}\rangle \langle \phi_i^{QP}| \right), \end{aligned} \quad (24)$$

where  $\hat{I}$  is the identity matrix. If we assume  $|\phi_i^{QP}\rangle \simeq |\phi_i^{KS}\rangle$ , Eq. (24) can be simplified

$$\hat{H}_{QP}^{\circ} = \hat{H}_{KS}^{\circ} + \sum_{i=1}^{n_{cut}} (|\phi_i^{KS}\rangle (\epsilon_i^{QP} - \epsilon_i^{KS} - \Delta) \langle \phi_i^{KS}|) + \Delta \hat{I}. \quad (25)$$

An alternative to the  $G_0W_0$  approach is the static COHSEX approximation. Although nonself-consistent COHSEX usually overestimates band gaps, a recent work suggests that band gaps obtained from the self-consistent static COHSEX (scCOHSEX) calculations may be more accurate than those computed using the  $G_0W_0$  approximation starting from LDA wave functions and, in some cases, of a quality comparable to those of self-consistent GW (scGW) calculations. For example, the  $G_0W_0$  gap of  $\text{Cu}_2\text{O}$  is 1.34 eV, while scGW (1.97 eV) and scCOHSEX (2.87 eV) results show better agreement with the experimental value of 2.17 eV.<sup>40,41</sup> Furthermore, using LDA wave functions,  $G_0W_0$  predicts the monoclinic  $\text{VO}_2$  to be metallic, in disagreement with a sizable gap of 0.6 eV observed experimentally, while the gaps predicted by scGW (0.65 eV) and scCOHSEX (0.78 eV) are consistent with experiment.<sup>43</sup> Finally, it has been shown that the scCOHSEX wave functions are a better approximation to the quasiparticle wave functions than the LDA wave functions.<sup>40,41,43,44</sup> Although there are not yet enough results available to assess the accuracy of the scCOHSEX approximation, the available ones are very promising.

Among the options for quasiparticle ground state calculations discussed above, the best choices would appear to be either the scCOHSEX or  $G_0W_0$  approaches, which are, however, computationally rather demanding. In particular, a *fully converged* GW calculation for molecules and nanostructures, in terms of the number of empty states and the dimension of  $\epsilon^{-1}(\mathbf{q}, \omega)$ , is highly nontrivial to carry out, and one would have to resort to newly developed algorithms, such as those proposed by Umari *et al.*<sup>45</sup> The latter approach is not yet interfaced with the code developed here to solve the BSE. For this reason, we used a simple “scissor” operator to approximate the self-energy correction. Work is in progress to implement more accurate approaches, such as scCOHSEX and  $G_0W_0$ .

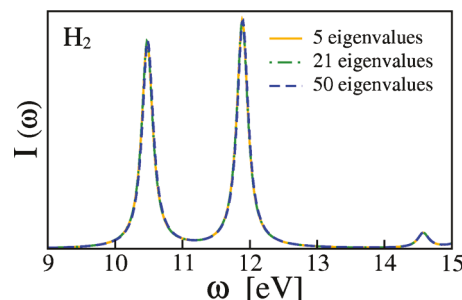


FIG. 1. Absorption spectrum of  $\text{H}_2$  computed by solving the Bethe-Salpeter equation and using 5, 21, and 50 eigenmodes to represent the dielectric matrix (see text).

The use of a scissor operator within a GW/BSE formalism has been discussed by several authors<sup>30,46,47</sup> and it is relatively well justified in *s-p* bonded solids, where self-energy corrections may be considered as rigid shifts of both LDA valence and conduction bands.<sup>46,47</sup> In molecules and nanoclusters, the use of a scissor operator approximation is expected to be less accurate, since self-energy corrections are likely to exhibit a stronger orbital dependence than in *s-p* bonded solids.<sup>30</sup> This is the case, for example, for systems with mixed degrees of localization in the valence and conduction electronic states. The effect of the scissor operator approximation in our calculations is discussed in the next section.

## IV. RESULTS

Our approach has been implemented in the software package QUANTUM ESPRESSO (Ref. 48) using plane wave basis sets and pseudopotentials. In all the calculations reported below, we do not truncate the basis set for either the dielectric matrix or the BSE kernel.

### A. Code verification

We first compared the absorption spectra of small molecules obtained with the algorithm of Sec. II with those computed with available codes using an electron-hole basis set. In particular, we compared with results obtained with the YAMBO code.<sup>23</sup> Since YAMBO uses the TDA, the same approximation was used in the calculations carried out with our code. The simplest case is the absorption spectrum of the  $\text{H}_2$  molecule provided as an example in the YAMBO tutorial.<sup>49</sup> The molecule was placed in a  $13.2 \times 13.2 \times 13.2 \text{ \AA}^3$  supercell. A kinetic energy cutoff of 28 Ry for the wave functions and a scissor operator of 7.6 eV were used, as given in the YAMBO tutorial. The matrix  $\tilde{\epsilon}^{-1}$  was decomposed into eigenvalues and eigenvectors according to Eq. (23). The eigenvectors of  $\tilde{\epsilon}^{-1}$  have 313 033 Fourier components, corresponding to the full potential cutoff (four times the wave function cutoff). Figure 1 shows the convergence of the spectrum of  $\text{H}_2$  as a function of the eigenmodes included in the summation in Eq. (23). The spectrum is fully converged by including only five eigenmodes, even though  $\lambda_5^{-1} - 1 = -0.16$  is still appreciably different from zero; for example, with 50 eigenmodes  $\lambda_{50}^{-1} - 1 = -0.01$ . In order to converge the YAMBO calculations with respect to the number of unoccupied elec-

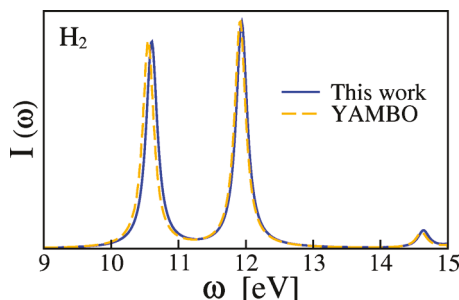


FIG. 2. Absorption spectrum of the  $\text{H}_2$  molecule obtained by solving the Bethe–Salpeter equation using the algorithm proposed in this work compared to that computed with the YAMBO code. The spectrum is given in arbitrary units and the Tamm–Dancoff approximation is used.

tronic states, we found it necessary to include 250 empty states to compute  $\tilde{\epsilon}^{-1}$  and 300 empty states to calculate the matrix elements of the BSE Hamiltonian. Due to memory limitations in the YAMBO code, the dimension of  $\tilde{\epsilon}^{-1}$  was truncated to  $10\,059 \times 10\,059$ , which corresponds to a cutoff of about 16 Ry. We note that even at the much higher energy cutoff (112 Ry corresponding to 313 033 Fourier components) used in our calculation, the storage of the five eigenpotentials necessary to represent  $\tilde{\epsilon}^{-1}$  takes only about 1.5% of the memory used in the YAMBO code, highlighting one of the advantages (memory saving) of the algorithm proposed here. As shown in Fig. 2, the results of the YAMBO code and of our code are in very good agreement, with differences smaller than 0.05 eV.

The second example chosen here is the silane molecule. The molecule is placed in a  $13.2 \times 13.2 \times 13.2 \text{ \AA}^3$  supercell and a kinetic energy cutoff of 20 Ry for the wave function is used. We adopted a scissor operator of 6.09 eV, from the COHSEX calculation of Ref. 17. The eigenvectors of  $\tilde{\epsilon}^{-1}$  have 189 047 Fourier components, corresponding to a cutoff of 80 Ry. Figure 3 shows the convergence of the spectrum of  $\text{SiH}_4$  as a function of eigenmodes included in the summation in Eq. (23). A good convergence is already reached by including 19 eigenmodes ( $\lambda_{19}^{-1} - 1 = -0.20$ ) as compared, e.g., to 58 eigenmodes ( $\lambda_{58}^{-1} - 1 = -0.05$ ). Similar to the case of  $\text{H}_2$ , we found that the convergence of the absorption spectrum as a function of the number of eigenmodes is rather fast and can be achieved even if  $|\lambda_i^{-1} - 1|$  is still appreciably different from zero. In order to converge the YAMBO calculations, we included 300 empty states to compute both  $\tilde{\epsilon}^{-1}$  and the BSE Hamiltonian. The size of  $\tilde{\epsilon}^{-1}$  was truncated to 10 059

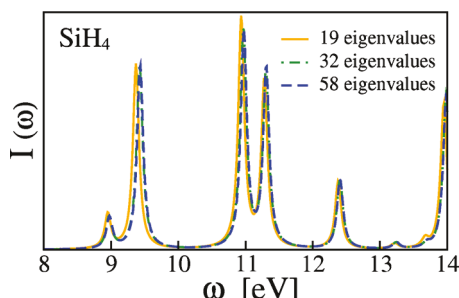


FIG. 3. Absorption spectrum of  $\text{SiH}_4$  computed by solving the Bethe–Salpeter equation and using 19, 32, and 58 eigenmodes to represent the dielectric matrix (see text).

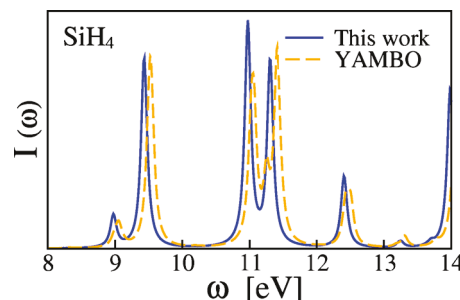


FIG. 4. Comparison between the absorption spectrum of the  $\text{SiH}_4$  molecule obtained by using the method proposed in this work and the YAMBO code. The spectrum is given in arbitrary units and the Tamm–Dancoff approximation is used.

$\times 10\,059$ , corresponding to a cutoff of about 16 Ry. Again, a 28-fold saving in the storage of  $\tilde{\epsilon}^{-1}$  was achieved using our algorithm. The comparison between the silane spectra obtained with two different techniques is shown in Fig. 4: the YAMBO spectrum is slightly blueshifted by less than 0.1 eV. The small discrepancy in the peak positions is likely related to technical details of our and YAMBO implementations, such as the cutoff for the BSE kernel.

Despite the approximation introduced by the use of a scissor operator, we obtain the first three excitations of silane at 8.97, 9.43, and 10.97 eV in fairly good agreement with the experimental values of 8.8, 9.7, and 10.7 eV.<sup>50</sup> The qualitative trend in oscillator strengths correctly matches that observed experimentally, with the transition at 8.97 eV having the smallest oscillator strength and the transition at 10.97 eV having the largest.

## B. Efficiency of the technique for computation of large systems

We now discuss the efficiency of the iterative algorithm developed here, for the calculation of the absorption spectrum of a relatively large system, over a wide energy range. In Fig. 5, we report the absorption spectrum of a 1 nm silicon cluster ( $\text{Si}_{35}\text{H}_{36}$ , 176 electrons) computed over a 20 eV energy range. The cluster was placed in a  $21.2 \times 21.2 \times 21.2 \text{ \AA}^3$  supercell. We used a plane wave cutoff of 20 Ry for the electronic wave functions and 80 Ry for  $\tilde{\epsilon}^{-1}$ , which was approximated by 379 eigenmodes. In this case, due to the large size of the system, a systematic test of convergence as a function of the number of eigenmodes was not straightforward to carry out; however, the value of  $\lambda_{379}^{-1} - 1 = -0.22$ , as compared to the smallest eigenvalues included in the cases of  $\text{H}_2$  and silane, indicates a reasonably good convergence. The value of the scissor operator (3.48 eV) was taken from the GW calculations of Ref. 30. We found that the differences in the oscillator strengths and in the peak positions (about 0.1 eV) are small in the lower part of the spectrum up to about 8 eV when using the TDA; however, the agreement with the full calculation worsens<sup>36</sup> at a higher energy. As already discussed in Sec. III, the TDA, while performing well for periodic systems, may not give reliable results for finite systems, where the contribution of the electron-hole antipairs cannot be discarded.<sup>35,36</sup> To the best of our knowledge, the results reported in Fig. 5(a) represent the first BSE

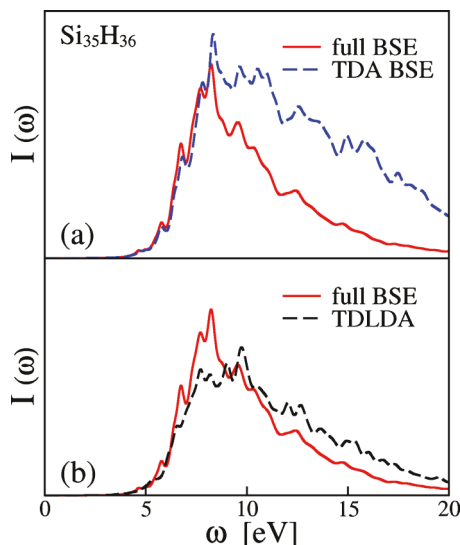


FIG. 5. (a) Absorption spectra in arbitrary units of a 1 nm silicon cluster obtained by solving the BSE (see text) with and without the TDA. A Lorentzian broadening of 0.14 eV was used. (b) Comparison of the BSE and TDLDA spectra of a 1 nm silicon cluster. A Lorentzian broadening of 0.14 eV was used.

calculations for a 1 nm Si cluster in such a wide energy range and the first calculation of such a system not employing the TDA. In Fig. 5(b), we compare the absorption spectra of the silicon nanocluster as obtained by solving the BSE and by using time-dependent DFT within the local density approximation (TDLDA). Although qualitatively similar, as pointed out in Refs. 29 and 30, the BSE and TDLDA spectra show quantitative differences in oscillator strengths in the lower part of the spectrum.

### C. Description of charge transfer excitations

We now turn to the study of a system exhibiting charge transfer (CT) excitations in its absorption spectrum. CT excitations are not only present in biological systems,<sup>51,52</sup> but also involved in, e.g., functionalized surfaces of photovoltaic cells.<sup>3</sup> The correct description of CT excitations requires the use of nonlocal exchange functionals and cannot be obtained, e.g., within time-dependent LDA or GGA.<sup>53</sup> On the other hand, the use of TDHF, although providing the correct asymptotic behavior of the exchange potential, generally leads to a poor description of electronic excitations, due to an overestimate of the electron-hole interaction because of the absence of screening. Since the BSE includes proper screening to the nonlocal exchange, it appears to be a promising framework to investigate CT excitations. The performance of BSE on CT excitations is practically unknown, as there has not yet been any application, primarily due to the high computational cost of conventional BSE implementations. In this study, we present the first application of the BSE to CT excitations and discuss the strengths and limitations of our approach.

We considered a model dipeptide molecule, consisting of two peptide groups ( $-\text{NHCO}-$ ) linked by an alkyl group ( $-\text{CH}_2-$ ) and terminated by methyl groups. In Fig. 6, we show the specific configuration (that corresponds to configu-

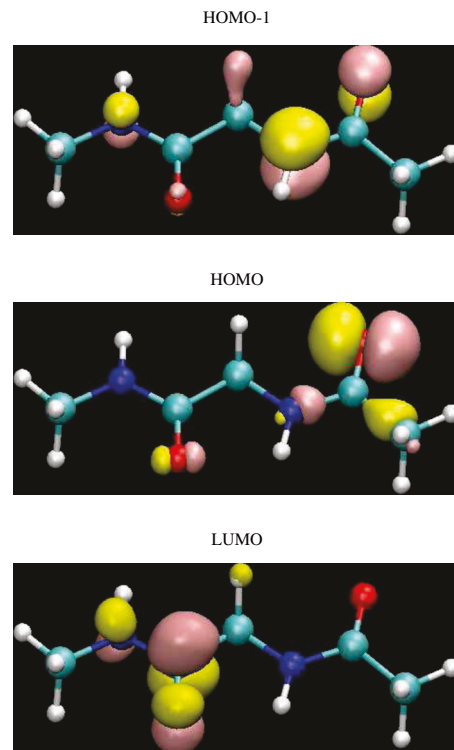


FIG. 6. HOMO, HOMO-1, and LUMO of the dipeptide molecule computed within LDA. The HOMO ( $n_1$ ) and HOMO-1 ( $\pi_1$ ) are localized on different peptides with respect to the LUMO ( $\pi_2^*$ ) and the transitions  $n_1 \rightarrow \pi_2^*$  and  $\pi_1 \rightarrow \pi_2^*$  have charge transfer character. Color code: white for hydrogen, light blue for carbon, blue for nitrogen, and red for oxygen.

ration 1a in Ref. 54) as well as three electronic orbitals, namely, the highest occupied molecular orbital (HOMO), HOMO-1, and the lowest unoccupied molecular orbital (LUMO).

Understanding the absorption spectrum of this simple model may help elucidate the features of the optical spectra of polypeptides; in addition, quantum chemistry results for portions of the spectrum are available at the complete active space multiconfigurational second order perturbation theory (CASPT2) level<sup>54,55</sup> and we will compare our findings with those results. The low energy spectrum of the model dipeptide is characterized by two local (L), weak intrapeptide excitations (namely, involving orbitals localized on the same peptide group) from oxygen  $n$  lone-pair orbitals to the  $\pi^*$  orbitals of the amides; these transitions are found at 5.62 and 5.79 eV by CASPT2 and have been assigned to the weak 5.7–5.8 eV band observed in the experimental spectra of polypeptides in solution.<sup>54</sup> The charge transfer excitations  $\pi_1 \rightarrow \pi_2^*$  and  $n_1 \rightarrow \pi_2^*$  between neighboring peptide units are found by CASPT2 at 7.18 and 8.07 eV, respectively. These excitations correspond to the HOMO-1  $\rightarrow$  LUMO and HOMO  $\rightarrow$  LUMO transitions and involve orbitals localized on different peptide groups (see Fig. 6). The CASPT2 results are consistent with the experimental findings; indeed a 7.2–7.6 eV band is found in the spectra of numerous polypeptides but, for example, not in nylons, where the peptide groups are separated by more than one alkyl group, and the probability of interpeptide transitions decreases significantly.<sup>54</sup> Compared to CASPT2 results, TDGGA generally accounts accu-

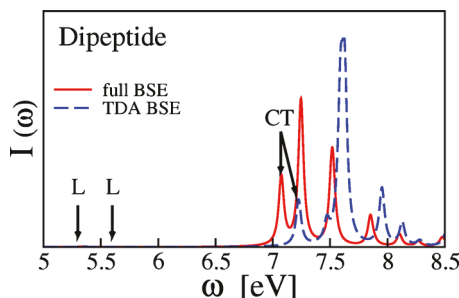


FIG. 7. Absorption spectra in arbitrary units of a model dipeptide obtained by solving the BSE (see text) with and without the TDA. A Lorentzian broadening of about 0.03 eV was used. The L and CT excitations are highlighted.

rately for the L excitations, with an error within 0.3 eV.<sup>55–57</sup> The CT excitation energies, however, are underestimated in TDGGA by about 2 and 3 eV, respectively,<sup>55,57</sup> and their relative position with respect to the local intrapeptide excitations is predicted incorrectly. The use of hybrid functionals, such as B3LYP, only partially improves over the TDGGA results<sup>55,57</sup> and the charge transfer excitations are still underestimated by about 1 and 2 eV, respectively.

In Fig. 7 and Table I, we present the spectra obtained in this work (with and without the TDA) and compare them with the CASPT2 results. The dipeptide was placed in a  $14.8 \times 14.8 \times 14.8 \text{ \AA}^3$  supercell and we used a 60 Ry kinetic energy cutoff for the electronic wave functions and a 240 Ry cutoff for  $\tilde{\epsilon}^{-1}$ ; 154 eigenmodes were used to approximate  $\tilde{\epsilon}^{-1}(\lambda_{154}^{-1} - 1 = -0.13)$ . Our TDLDA calculation predicts CT excitations at 4.61 and 5.16 eV and L excitations at 5.30 and 5.66 eV (in agreement with the TDGGA results in the literature). Since TDLDA accurately accounts for the peak position of local excitations, we choose the value of the scissor by aligning the first L excitation in the BSE and TDLDA spectra. The quality of the BSE in describing CT excitations can be evaluated by comparing the peak positions of the CT excitations to those obtained at the CASPT2 level. We found that the  $\pi_1 \rightarrow \pi_2^*$  peak (7.05 eV) is blueshifted by 1.9 eV in the full BSE, with respect to TDLDA, in good agreement with the CASPT2 result of 7.18 eV. The use of the TDA introduces a blueshift of 0.15 eV in the BSE results; quantitatively similar differences between TDA and BSE excitation energies were found in the case of molecules such as *trans*-azobenzene<sup>36</sup> and biological chromophores.<sup>35</sup> Due to the small oscillator strength, the  $n_1 \rightarrow \pi_2^*$  transition could not be identified in our BSE spectra, which is consistent with the

finding that this transition has zero oscillator strength (0.000) in the CASPT2 calculations.<sup>54</sup> From both Table I and Fig. 7, one notices that the TDA and the full BSE results are in qualitative agreement, although important quantitative differences exist. A discussion about the limitations of the TDA has already been given in Secs. III and IV B.

In Table I, we report the peak positions of the dipeptide spectrum, as obtained from direct diagonalization of the BSE Hamiltonian in an e-h pair basis set. This calculation allowed us to test the convergence properties of the e-h approach, compare the characteristics of the different methods, and assign the first few peaks in the excitation spectrum. In order to have a straightforward comparison of the results from the e-h approach and our method, we used our own implementation of the e-h algorithm based on  $\tilde{\epsilon}^{-1}$  as defined in Eq. (23). In particular, we found a slow convergence of the CT excitation energies as a function of  $N_c$ , the number of empty states. For example, although  $\pi_1 \rightarrow \pi_2^*$  is the third lowest excitation in BSE, the use of at least 154 empty states is necessary to obtain a 0.1 eV accuracy in the peak position. Including 214 empty states slightly improves the accuracy to 0.08 eV. In the low energy part of an absorption spectrum (like in this case), the convergence with respect to the number of e-h pairs could be hindered by the strong mixing of single particle transitions induced by the electron-hole interaction. In the high energy part of a spectrum, the electron-hole interaction is supposed to decrease but the density of single particle transitions in a given energy range increases, making the convergence with respect to the number of e-h pairs difficult. By reformulating the problem within density matrix perturbation theory, this basis set error is eliminated, as we include implicitly all the single particle empty states below the wave function kinetic energy cutoff. In the e-h approach, we found that the peak position of the  $n_1 \rightarrow \pi_2^*$  transition (7.37 eV) is blueshifted by 2.8 eV with respect to TDLDA. Although showing a large improvement over TDLDA, the peak position found by our BSE code is still 0.7 eV lower than the CASPT2 result, which may be attributed to the approximate nature of the scissor operator used here. This implies that the self-energy correction to the occupied states (or empty states) is not constant, but have a strong orbital dependence. It is also possible that the order of the KS electronic states is not preserved in the quasiparticle picture. This issue may be fixed by using state dependent  $G_0W_0$  or scCOHSEX corrections.

TABLE I. Transition energies of a model dipeptide molecule computed from TDLDA and BSE compared to CASPT2 results. The indices 1 and 2 indicate orbital localized on different peptides. The transitions that do not significantly contribute to the spectrum in Fig. 7, namely, whose oscillator strength is approximately zero, are indicated with o.s.  $\approx 0$  (the negligible oscillator strength found by our BSE code is in agreement with CASPT2 results).

Optical excitation	TDLDA (TDA)	TDLDA	BSE-e-h <sup>a</sup> (TDA)	BSE-e-h <sup>b</sup> (TDA)	BSE (TDA)	BSE	CASPT2 <sup>c</sup>
$n_1 \rightarrow \pi_2^*$ (CT)	4.61	4.61	7.38	7.37	o.s. $\approx 0$	o.s. $\approx 0$	8.07
$\pi_1 \rightarrow \pi_2^*$ (CT)	5.16	5.15	7.30	7.28	7.20	7.05	7.18
$n_1 \rightarrow \pi_1^*$ (L)	5.30	5.30	5.38	5.37	5.33	5.30	5.62
$n_2 \rightarrow \pi_2^*$ (L)	5.67	5.66	5.67	5.66	5.63	5.60	5.79

<sup>a</sup>154 empty states are used in the e-h pair basis set.

<sup>b</sup>214 empty states are used in the e-h pair basis set.

<sup>c</sup>Reference 54.

In addition to the L and CT transitions, local  $\pi \rightarrow \pi^*$  intense excitations (called NV<sub>1</sub> excitations) are also present in the dipeptide spectrum. These are found at 6.39 and 6.49 eV within CASPT2, in reasonable agreement with the experimental results for polypeptides; indeed, an intense band at 6.4–6.7 eV is typically observed for peptides ranging from small amides to large polymers.<sup>54</sup> An accurate description of such transitions remains quite challenging. For example, compared with CASPT2, TDGGA overestimates the NV<sub>1</sub> excitations by more than 0.5 eV and TDB3LYP by almost 1 eV.<sup>55</sup> The CAM-B3LYP [a range-separated hybrid functional using the Coulomb-attenuating method (CAM) that improves over B3LYP in describing the CT excitations in the dipeptide model, however, when compared to CASPT2 (Refs. 56 and 57)] overestimates the NV<sub>1</sub> transitions by 0.34 eV.<sup>56</sup> In our calculation, we did not find NV<sub>1</sub> excitations in the energy range predicted by CASPT2, similar to the trend in TDGGA<sup>55,57</sup> and TDB3LYP/CAM-B3LYP.<sup>55,57</sup> These excitations are shifted to higher energies in BSE, where many transitions are present, making it difficult to clearly identify the nature of the peaks within our approach. From the direct diagonalization of the e-h BSE Hamiltonian (TDA), NV<sub>1</sub> transitions are found at 7.98 and 8.24 eV when including 154 empty states and at 7.88 and 7.67 eV when including 214 empty states. Due to the slow convergence of calculations using the e-h hole basis, it is difficult to accurately assign NV<sub>1</sub> transitions in Fig. 7. In principle, this would be possible by direct diagonalization of the Liouvillian operator  $\mathcal{L}$ , but this has not yet been implemented in our code. A method to assign transitions in an implementation similar to ours has been introduced in Ref. 58. However, in order to assign a single transition of energy  $\omega$ , this approach requires an additional iterative calculation with a computational cost comparable to the calculation of the full spectrum.

Multiple factors may be responsible for the poor description of the NV<sub>1</sub> transitions in our BSE spectra and the exact reasons are yet unclear. A substantial source of error might come from the use of the same scissor operator to account for the self-energy correction of different excitations. A fully self-consistent self-energy calculation, at least at the COHSEX level, would be necessary to improve over the use of a constant scissor shift and work is in progress to carry out such a computation. On the other hand, theoretical studies of the NV transition of N-methylacetamide, the monomer of the dipeptide studied here, have not reached a consensus on the position of NV transitions. While the  $\pi \rightarrow \pi^*$  excitation is at 6.76 eV in CASPT2,<sup>59</sup> in good agreement with the experimental result of 6.8 eV,<sup>60</sup> multireference configuration interaction (MRCI) calculations obtained a value at 7.46 eV, about 0.8 eV higher than experiment.<sup>61</sup> Clearly, the MRCI calculation shows the same trend as our BSE calculation, namely, a significant blueshift of the NV<sub>1</sub> transition. The discrepancy between CASPT2 and MRCI has been attributed to the different treatment of the valence-Rydberg state mixing.<sup>59,61</sup> Hirst *et al.*<sup>61</sup> also argued that the NV excitation observed in experiments may not be a vertical transition, similar to the case of ethylene. Therefore, it is not yet clear if the discrepancy between BSE and CASPT2 results mainly

stems from approximations in our implementations, e.g., the use of a constant scissor operator, or from other issues, such as the valence-Rydberg state mixing.

## V. CONCLUSIONS

In conclusion, we have introduced a new *ab initio* approach to compute the optical absorption spectra of molecules and solids by solving the BSE, whose computational workload is comparable to ground state Hartree–Fock calculations. Within the framework presented here, explicit calculations of empty states and inversion of dielectric matrices are avoided; the efficiency of our method for relatively large systems was demonstrated for a 1 nm size silicon cluster. We also applied the new approach to a model dipeptide molecule that exhibits charge transfer excitations. Work is in progress to improve the accuracy of the method through the introduction of quasiparticle corrections to single particle electronic states.

## ACKNOWLEDGMENTS

This work was supported by NSF CHE-0802907 grant and DOE BES-FG02-06ER46262 grant and computer time was provided by NERSC and Teragrid. We thank Luis Serrano-Andrés and Stefano Baroni for useful discussions. D.L. thanks Conor Hogan and Andrea Marini for their help with the YAMBO code.

## APPENDIX: GENERALIZATION TO EXTENDED SYSTEMS

Here we briefly present the generalization of the formalism of Sec. II to extended systems. The optical absorption spectrum of a solid is given by the imaginary part of the macroscopic dielectric function  $\epsilon_2$ ; following Ref. 2 [Eqs. 2.23 and B26],

$$\epsilon_2(\omega) = - \lim_{\mathbf{q} \rightarrow 0} v(\mathbf{q}) \text{Im} \left( \sum_{n_1, n_2} \sum_{n_3, n_4} \langle \phi_{n_1}^\circ | e^{-i\mathbf{q} \cdot \mathbf{r}} | \phi_{n_2}^\circ \rangle \times (\omega - \mathcal{L} + i\eta)_{n_1 n_2, n_3 n_4}^{-1} \langle \phi_{n_4}^\circ | e^{i\mathbf{q} \cdot \mathbf{r}'} | \phi_{n_3}^\circ \rangle (f_{n_3} - f_{n_4}) \right), \quad (\text{A1})$$

where  $v(\mathbf{q}) = 4\pi/q^2$  is the Coulomb potential in Fourier space and  $f_{n_i}$  are the occupation numbers of the quasiparticle orbitals  $\phi_{n_i}^\circ$ . In the long wavelength limit, the exponential  $e^{-i\mathbf{q} \cdot \mathbf{r}}$  can be expanded into powers of  $\mathbf{q}$ ,

$$\lim_{\mathbf{q} \rightarrow 0} \langle \phi_{n_i}^\circ | \frac{e^{-i\mathbf{q} \cdot \mathbf{r}}}{q} | \phi_{n_j}^\circ \rangle = -i \langle \phi_{n_i}^\circ | \vec{e} \cdot \mathbf{r} | \phi_{n_j}^\circ \rangle, \quad (\text{A2})$$

where  $\vec{e}$  is the polarization direction of the external field and the orthogonality between  $|\phi_{n_i}^\circ\rangle$  and  $|\phi_{n_j}^\circ\rangle$  is used. By substituting Eq. (A2) into Eq. (A1), we obtain

$$\epsilon_2(\omega) = -4\pi Im \left( \sum_{n_1, n_2} \sum_{n_3, n_4} \langle \phi_{n_1}^\circ | \vec{e} \cdot \mathbf{r} | \phi_{n_2}^\circ \rangle \times (\omega - \mathcal{L} + i\eta)_{n_1 n_2; n_3 n_4}^{-1} \langle \phi_{n_4}^\circ | \vec{e} \cdot \mathbf{r}' | \phi_{n_3}^\circ \rangle (f_{n_3} - f_{n_4}) \right). \quad (A3)$$

It is straightforward to see that this equation is equivalent, but for a constant factor  $4\pi$ , to the imaginary part of Eq. (6); indeed  $\langle \phi_{n_1}^\circ | \vec{e} \cdot \mathbf{r} | \phi_{n_2}^\circ \rangle$  is the e-h hole representation of  $\vec{e} \cdot \mathbf{r}$  and  $\langle \phi_{n_4}^\circ | \vec{e} \cdot \mathbf{r}' | \phi_{n_3}^\circ \rangle (f_{n_3} - f_{n_4})$  corresponds to the commutator  $[\vec{e} \cdot \mathbf{r}', \hat{\rho}^\circ]$ .

The calculation of optical spectra of periodic systems requires the evaluation of a properly converged integral over the first Brillouin zone (BZ) and we note that each single particle state is labeled by wave vector indices  $\mathbf{k}$ , belonging to the first BZ.

- <sup>1</sup>P. Y. Yu and M. Cardona, *Fundamentals of Semiconductors: Physics and Material Properties* (Springer, New York, 1996).
- <sup>2</sup>G. Onida, L. Reining, and A. Rubio, *Rev. Mod. Phys.* **74**, 601 (2002).
- <sup>3</sup>M. K. Nazeeruddin, F. De Angelis, S. Fantacci, A. Selloni, G. Viscardi, P. Liska, S. Ito, B. Takeru, and M. Grätzel, *J. Am. Chem. Soc.* **127**, 16835 (2005).
- <sup>4</sup>B. M. Kayes, M. A. Filler, M. C. Putnam, M. D. Kelzenberg, N. S. Lewis, and H. A. Atwater, *Appl. Phys. Lett.* **91**, 103110 (2007).
- <sup>5</sup>E. C. Garnett and P. Yang, *J. Am. Chem. Soc.* **130**, 9224 (2008).
- <sup>6</sup>E. Runge and E. K. U. Gross, *Phys. Rev. Lett.* **52**, 997 (1984).
- <sup>7</sup>M. Rohlfing and S. G. Louie, *Phys. Rev. B* **62**, 4927 (2000).
- <sup>8</sup>W. Kohn and L. J. Sham, *Phys. Rev.* **140**, A1133 (1965).
- <sup>9</sup>L. Hedin, *Phys. Rev.* **139**, A796 (1965).
- <sup>10</sup>P. H. Hahn, W. G. Schmidt, K. Seino, M. Preuss, F. Bechstedt, and J. Bernholc, *Phys. Rev. Lett.* **94**, 037404 (2005).
- <sup>11</sup>V. Garbuio, M. Casella, L. Reining, R. Del Sole, and O. Pulci, *Phys. Rev. Lett.* **97**, 137402 (2006).
- <sup>12</sup>L. Yang, J. Deslippe, C.-H. Park, M. L. Cohen, and S. G. Louie, *Phys. Rev. Lett.* **103**, 186802 (2009).
- <sup>13</sup>C. D. Spataru, S. Ismail-Beigi, L. X. Benedict, and S. G. Louie, *Phys. Rev. Lett.* **92**, 077402 (2004).
- <sup>14</sup>L. Wirtz, A. Marini, and A. Rubio, *Phys. Rev. Lett.* **96**, 126104 (2006).
- <sup>15</sup>G. Onida, L. Reining, R. W. Godby, R. del Sole, and W. Andreoni, *Phys. Rev. Lett.* **75**, 818 (1995).
- <sup>16</sup>M. L. Tiago and J. R. Chelikowsky, *Solid State Commun.* **136**, 333 (2005).
- <sup>17</sup>P. H. Hahn, W. G. Schmidt, and F. Bechstedt, *Phys. Rev. B* **72**, 245425 (2005).
- <sup>18</sup>S. Baroni, S. de Gironcoli, A. Dal Corso, and P. Giannozzi, *Rev. Mod. Phys.* **73**, 515 (2001).
- <sup>19</sup>H. F. Wilson, F. Gygi, and G. Galli, *Phys. Rev. B* **78**, 113303 (2008).
- <sup>20</sup>H. F. Wilson, D. Lu, F. Gygi, and G. Galli, *Phys. Rev. B* **79**, 245106 (2009).
- <sup>21</sup>B. Walker, A. M. Saitta, R. Gebauer, and S. Baroni, *Phys. Rev. Lett.* **96**, 113001 (2006).
- <sup>22</sup>D. Rocca, R. Gebauer, Y. Saad, and S. Baroni, *J. Chem. Phys.* **128**, 154105 (2008).
- <sup>23</sup>A. Marini, C. Hogan, M. Grüning, and D. Varsano, *Comput. Phys. Commun.* **180**, 1392 (2009).
- <sup>24</sup>D. Rocca, R. Gebauer, F. De Angelis, M. K. Nazeeruddin, and S. Baroni, *Chem. Phys. Lett.* **475**, 49 (2009).
- <sup>25</sup>L. Huang, D. Rocca, S. Baroni, K. E. Gubbins, and M. B. Nardelli, *J. Chem. Phys.* **130**, 194701 (2009).
- <sup>26</sup>A. Gali, M. Voros, D. Rocca, G. Zimanyi, and G. Galli, *Nano Lett.* **9**, 3780 (2009).
- <sup>27</sup>R. Car, E. Tosatti, S. Baroni, and S. Leelaprate, *Phys. Rev. B* **24**, 985 (1981).
- <sup>28</sup>L. X. Benedict, E. L. Shirley, and R. B. Bohn, *Phys. Rev. Lett.* **80**, 4514 (1998).
- <sup>29</sup>L. X. Benedict, A. Puzder, A. J. Williamson, J. C. Grossman, G. Galli, J. E. Klepeis, J.-Y. Raty, and O. Pankratov, *Phys. Rev. B* **68**, 085310 (2003).
- <sup>30</sup>M. L. Tiago and J. R. Chelikowsky, *Phys. Rev. B* **73**, 205334 (2006).
- <sup>31</sup>I. Tamm, *J. Phys. (Moscow)* **78**, 382 (1945).
- <sup>32</sup>S. Albrecht, G. Onida, and L. Reining, *Phys. Rev. B* **55**, 10278 (1997).
- <sup>33</sup>S. Albrecht, L. Reining, R. Del Sole, and G. Onida, *Phys. Rev. Lett.* **80**, 4510 (1998).
- <sup>34</sup>V. Olevano and L. Reining, *Phys. Rev. Lett.* **86**, 5962 (2001).
- <sup>35</sup>Y. Ma, M. Röhlffing, and C. Molteni, *Phys. Rev. B* **80**, 241405 (2009).
- <sup>36</sup>M. Grüning, A. Marini, and X. Gonze, *Nano Lett.* **9**, 2820 (2009).
- <sup>37</sup>K. Shindo, *J. Phys. Soc. Jpn.* **29**, 287 (1970).
- <sup>38</sup>F. Bechstedt, F. Rödl, L. E. Ramos, F. Fuchs, P. H. Hahn, and J. Furthmüller, in *Epioptrics-9: Proceedings of the 39th Course of the International School of Solid State Physics*, Erice, Italy, 20–26 July 2006, edited by A. Criventi (World Scientific, Singapore, 2006), pp. 28–40.
- <sup>39</sup>M. van Schilfgaarde, T. Kotani, and S. Faleev, *Phys. Rev. Lett.* **96**, 226402 (2006).
- <sup>40</sup>F. Bruneval, Ph.D. thesis, École Polytechnique, Palaiseau, France, 2005. Available at [http://theory.lsi.polytechnique.fr/people/bruneval/bruneval\\_these.pdf](http://theory.lsi.polytechnique.fr/people/bruneval/bruneval_these.pdf).
- <sup>41</sup>F. Bruneval, N. Vast, L. Reining, M. Izquierdo, F. Sirotti, and N. Barrett, *Phys. Rev. Lett.* **97**, 267601 (2006).
- <sup>42</sup>Dependence of  $G_0W_0$  results on the single particle wave functions used as input have been investigated, for example, in Refs. 62 and 63.
- <sup>43</sup>M. Gatti, F. Bruneval, V. Olevano, and L. Reining, *Phys. Rev. Lett.* **99**, 266402 (2007).
- <sup>44</sup>F. Bruneval, N. Vast, and L. Reining, *Phys. Rev. B* **74**, 045102 (2006).
- <sup>45</sup>P. Umari, G. Stenuit, and S. Baroni, *Phys. Rev. B* **81**, 115104 (2010).
- <sup>46</sup>M. S. Hybertsen and S. G. Louie, *Phys. Rev. B* **34**, 5390 (1986).
- <sup>47</sup>W. G. Aulbur, L. Jönsson, and J. W. Wilkins, *Solid State Phys.* **54**, 1 (1999).
- <sup>48</sup>P. Giannozzi, S. Baroni, N. Bonini, M. Calandra, R. Car, C. Cavazzoni, D. Ceresoli, G. L. Chiarotti, M. Cococcioni, I. Dabo, A. Dal Corso, S. de Gironcoli, S. Fabris, G. Fratesi, R. Gebauer, U. Gerstmann, C. Gougoussis, A. Kokalj, M. Lazzeri, L. Martin-Samos, N. Marzari, F. Mauri, R. Mazzarello, S. Paolini, A. Pasquarello, L. Paulatto, C. Sbraccia, S. Scandolo, G. Sclauzero, A. P. Seitsonen, A. Smogunov, P. Umari, and R. M. Wentzcovitch, *J. Phys.: Condens. Matter* **21**, 395502 (2009).
- <sup>49</sup>See <http://www.yambo-code.org/> for the download and documentation of the Yambo code.
- <sup>50</sup>U. Itoh, Y. Toyoshima, H. Onuki, N. Washida, and T. Ibuki, *J. Chem. Phys.* **85**, 4867 (1986).
- <sup>51</sup>A. Drew and M. Head-Gordon, *J. Am. Chem. Soc.* **126**, 4007 (2004).
- <sup>52</sup>A. Drew, G. F. Fleming, and M. Head-Gordon, *J. Phys. Chem. B* **107**, 6500 (2003).
- <sup>53</sup>A. Drew, J. L. Weisman, and M. Head-Gordon, *J. Chem. Phys.* **119**, 2943 (2003).
- <sup>54</sup>L. Serrano-Andrés and M. Fulscher, *J. Am. Chem. Soc.* **120**, 10912 (1998).
- <sup>55</sup>D. J. Tozer, R. D. Amos, N. C. Handy, B. O. Roos, and L. Serrano-Andrés, *Mol. Phys.* **97**, 859 (1999).
- <sup>56</sup>T. Yanai, D. P. Tew, and N. C. Handy, *Chem. Phys. Lett.* **393**, 51 (2004).
- <sup>57</sup>M. J. G. Peach, P. Benfield, T. Helgaker, and D. J. Tozer, *J. Chem. Phys.* **128**, 044118 (2008).
- <sup>58</sup>L. X. Benedict and E. L. Shirley, *Phys. Rev. B* **59**, 5441 (1999).
- <sup>59</sup>L. Serrano-Andrés and M. Fulscher, *J. Am. Chem. Soc.* **118**, 12190 (1996).
- <sup>60</sup>K. Kaya and S. Nakagura, *Theor. Chim. Acta* **7**, 117 (1967).
- <sup>61</sup>J. D. Hirst, D. M. Hirst, and C. L. Brooks III, *J. Phys. Chem. A* **101**, 4821 (1997).
- <sup>62</sup>F. Fuchs, J. Furthmüller, F. Bechstedt, M. Shishkin, and G. Kresse, *Phys. Rev. B* **76**, 115109 (2007).
- <sup>63</sup>C. Rödl, F. Fuchs, J. Furthmüller, and F. Bechstedt, *Phys. Rev. B* **79**, 235114 (2009).